Chemical Engineering Science 146 (2016) 357–368

Contents lists available at ScienceDirect

Chemical Engineering Science

journal homepage: www.elsevier.com/locate/ces

Simple method for measuring the spectral absorption cross-section of microalgae

Razmig Kandilian [a,b], Antoine Soulies [b], Jeremy Pruvost [b], Benoit Rousseau [c], Jack Legrand [b], Laurent Pilon [a,*]

[a] Mechanical and Aerospace Engineering Department, Henry Samueli School of Engineering and Applied Science, University of California, 420 Westwood Plaza, Eng. IV 37-132, Los Angeles, CA 90095, USA
[b] Université de Nantes, GEPEA CNRS, UMR 6144, Bd de l'Université, CRTT - BP 406, 44602 Saint-Nazaire Cedex, France
[c] Laboratoire de Thermocinétique de Nantes, Université de Nantes, UMR CNRS 6607, Nantes, France

HIGHLIGHTS

- A simple procedure for measuring microalgae spectral absorption cross-section is proposed.
- It is based on normal–hemispherical transmittance and reflectance measurements.
- It was validated against direct measurements of the radiation characteristics of *C. vulgaris*.
- It can be used for other suspensions of absorbing and scattering particles.
- It can be used to predict and control light transfer and biomass productivity in PBRs.

ARTICLE INFO

Article history:
Received 15 October 2015
Received in revised form
16 February 2016
Accepted 23 February 2016
Available online 3 March 2016

Keywords:
Light transfer
Photobioreactors
Light absorption
Microalgae
Growth modeling

ABSTRACT

The spectral absorption cross-section of microalgae is an essential parameter in modeling the microalgae metabolism and growth kinetics as well as in estimating the productivity and efficiency of photobioreactors. This paper presents a simple experimental procedure for retrieving the average spectral absorption cross-section of concentrated microalgal suspensions. The method combines experimental measurements of the normal–hemispherical transmittance and reflectance of the suspensions in conventional cuvettes with an inverse method and analytical expressions obtained from the modified two-flux approximation accounting for absorption and multiple scattering. The method was validated with direct measurements of the scattering phase function and of the absorption and scattering cross-sections of freshwater microalgae *Chlorella vulgaris*. It was able to retrieve the absorption cross-section with acceptable accuracy. The latter was then used to estimate successfully the fluence rate using a simplified light transfer model, the local rate of photon absorption, and the biomass productivity in flat plate PBRs.

1. Introduction

Cultivation of photosynthetic microorganisms has received significant interest in recent years as a way to produce a broad range of chemical compounds including food supplements, fertilizers, hydrogen gas, and lipids for biodiesel production (Richmond, 2004). A wide variety of microalgae and cyanobacteria species can be cultivated in fresh or brackish waters as well as in seawater. Cultivation typically takes place in outdoor raceway ponds or photobioreactors. Light transfer in such systems is arguably one of the most important parameters affecting both the growth rate and metabolism of the photosynthetic microorganisms (Cornet et al., 1998; Pilon et al., 2011). Illumination conditions within the culture can vary strongly with time depending on the season, on the local weather, and on the photoadaptation of the microorganisms which reduces or increases their pigment concentrations under excessive illumination or light limiting conditions, respectively. Physical modeling coupling light transfer to growth kinetics and metabolic activities can facilitate the optimum design, operation, and control of photobioreactors (Cornet et al., 1992, 1992, 1995; Cornet and Dussap, 2009; Murphy and Berberoğlu, 2011; Pilon et al., 2011; Takache et al., 2010, 2012; Pruvost et al., 2012; Wheaton and Krishnamoorthy, 2012; Kandilian et al., 2014; Kong and Vigil, 2014). To do so, knowing the radiation characteristics of microalgae and the amount of light they absorb to drive the photosynthesis is essential. In fact, the radiation characteristics of microorganisms vary significantly among species (Berberoğlu and Pilon,

* Corresponding author. Tel.: +1 310 206 5598; fax: +1 310 206 2302.
E-mail address: pilon@seas.ucla.edu (L. Pilon).

http://dx.doi.org/10.1016/j.ces.2016.02.039
0009-2509/

2007; Berberoğlu et al., 2008; Heng et al., 2014) or during the cultivation process. This is particularly true during nitrogen starvation used to trigger lipid accumulation (Kandilian et al., 2013; Heng et al., 2014; Heng and Pilon, 2014; Kandilian et al., 2014).

The goal of the present study is to develop a simple yet accurate experimental method for determining the spectral absorption cross-section of microalgae over the photosynthetically active radiation (PAR) region, corresponding to wavelength between 400 and 700 nm. This method does not require the knowledge of the scattering phase function of the microorganisms or the use of a nephelometer, which can be costly and difficult to operate. Moreover, it only requires an integrating sphere spectrophotometer. It also aims to demonstrate that the use of the absorption cross-section alone with a simplified light transfer model is sufficient to predict light transfer, growth kinetics, and biomass productivity of PBRs. The unicellular microalgae *Chlorella vulgaris* was used to illustrate the new method because of the interest in the wide range of compounds it can produce.

2. Background

2.1. Chlorella vulgaris

Chlorella vulgaris is a unicellular microalgae with spherical shape and 1–6 μm in diameter (Safi et al., 2014). This particular species of green microalgae has garnered special attention for its large areal biomass productivity and its relatively short cell doubling time (Griffiths and Harrison, 2009). In addition, it has been identified as a potential source of protein for human and animal feed (Tokuşoglu and Ünal, 2003). It is also an important source for the commercial production of carotenoids and various biopharmaceuticals (Mendes et al., 2003). It can also produce lipids to be converted into biodiesel (Brennan and Owende, 2003). Finally, this freshwater species can be cultivated in wastewater for simultaneous wastewater treatment and production of value-added products (Feng et al., 2011).

2.2. One-dimensional radiative transfer equation

Fig. 1 shows a schematic of a microalgae suspension of thickness ℓ illuminated with collimated, unpolarized, and normally incident light along with the associated coordinate system. Light transfer through such absorbing, anisotropically scattering, and non-emitting suspension can be treated as one-dimensional (1D) along the z-direction taken as the direction of the incident light. It is governed by the 1D radiation transfer equation (RTE) expressed in terms of the local spectral light intensity $I_\lambda(\mu,z)$ (in W/m^2 sr μm) at location z, in direction θ, and at wavelength λ as (Modest, 2013),

$$\mu\frac{\partial I_\lambda}{\partial z}=-(\kappa_\lambda+\sigma_{s,\lambda})I_\lambda+\frac{\sigma_{s,\lambda}}{2}\int_{-1}^{1}p_\lambda(\mu',\mu)I_\lambda(\mu',z)\mathrm{d}\mu' \tag{1}$$

where $\mu=\cos\theta$ is the direction cosine, κ_λ and $\sigma_{s,\lambda}$ are respectively the absorption and scattering coefficients while $p_\lambda(\mu',\mu)$ is the azimuthally symmetric scattering phase function. The latter represents the probability that photons coming from direction $\mu'=\cos\theta'$ be scattered in direction $\mu=\cos\theta$. It is normalized such that

$$\frac{1}{2}\int_{-1}^{1}p_\lambda(\mu',\mu)\,\mathrm{d}\mu'=1. \tag{2}$$

For the azimuthally symmetric problem, $p_\lambda(\mu',\mu)$ depends only on $\mu_0=\cos\theta_0$ where θ_0 is the angle between the radiation incident on the scatterer along direction $\mu'=\cos\theta'$ and the intensity scattered in direction $\mu=\cos\theta$, i.e., $p_\lambda(\mu',\mu)=p_\lambda(\mu_0)$. From geometrical consideration, μ_0 can be expressed as $\mu_0=\mu\mu'+(1-\mu^2)^{1/2}(1-\mu'^2)^{1/2}$ (Modest, 2013).

In cases when scatterers are much larger than the radiation wavelength, scattering is mainly forward and the scattering phase function can be estimated based on the transport approximation as $p_\lambda(\mu_0)=1-g_\lambda+2g_\lambda\delta(1-\mu_0)$ (McKellar and Box, 1981). Here, $\delta(\mu)$ is the Dirac delta function and g_λ is the asymmetry factor at wavelength λ defined as

$$g_\lambda=\frac{1}{2}\int_{-1}^{1}p_\lambda(\mu_0)\mu_0\,\mathrm{d}\mu_0. \tag{3}$$

Then, the RTE can be expressed as

$$\mu\frac{\partial I_\lambda}{\partial z}=-(\kappa_\lambda+\sigma_{s,tr,\lambda})I_\lambda+\frac{\sigma_{s,tr,\lambda}}{2}\int_{-1}^{1}I_\lambda(\mu',z)\mathrm{d}\mu' \tag{4}$$

where $\sigma_{s,tr,\lambda}=(1-g_\lambda)\sigma_{s,\lambda}$ is the transport scattering coefficient.

In the context of light transfer in photobioreactors, the absorption and scattering coefficients are linearly proportional to the number density N_T of the microalgae cells (in #/m^3) and expressed as

$$\kappa_\lambda=\overline{C}_{abs,\lambda}N_T \quad\text{and}\quad \sigma_{s,\lambda}=\overline{C}_{sca,\lambda}N_T \tag{5}$$

where $\overline{C}_{abs,\lambda}$ and $\overline{C}_{sca,\lambda}$ (in m^2) are the average spectral absorption and scattering cross-sections of a cell, respectively. Alternatively, the biomass concentration of the microalgal suspension X, expressed in mass of dry weight per unit volume (g/L or kg/m^3), is often measured instead of N_T. Then, one can express κ_λ and $\sigma_{s,\lambda}$ as

$$\kappa_\lambda=\overline{A}_{abs,\lambda}X \quad\text{and}\quad \sigma_{s,\lambda}=\overline{S}_{sca,\lambda}X \tag{6}$$

where $\overline{A}_{abs,\lambda}$ and $\overline{S}_{sca,\lambda}$ are the average spectral mass absorption and scattering cross-sections expressed in m^2/kg dry weight. Typically, the biomass concentration X in conventional PBR vary from 0.1 to 2.0 kg/m^3 (Takache et al., 2010).

2.3. Fluence rate

The local spectral fluence rate $G_\lambda(z)$ in a PBR is defined as the irradiance incident at location z from all directions. It is expressed in W/m^2 μm or μmol$_{h\nu}$/m^2 s μm and defined, in 1D radiation transfer, as

$$G_\lambda(z)=2\pi\int_{-1}^{1}I_\lambda(z,\mu)\,\mathrm{d}\mu. \tag{7}$$

Cornet and co-workers solved the above 1D RTE using the Schuster–Schwarzschild two-flux approximation to predict the local fluence rate $G_\lambda(z)$ in flat plate PBR illuminated on one side with a black (Cornet et al., 1992) or diffusely reflecting (Pottier et al., 2005) wall on the other. Their solution accounted for multiple and anisotropic scattering. For example, the local fluence rate $G_\lambda(z)$ in a flat plate PBR with a transparent front window and a diffusely reflecting back wall of reflectance ρ_λ exposed to collimated spectral irradiance $q''_{in,\lambda}$ normally incident onto the photobioreactor as (Pottier et al., 2005),

$$G_\lambda(z)=2q''_{in,\lambda}\frac{[\rho_\lambda(1+\alpha_\lambda)e^{-\delta_\lambda L}-(1-\alpha_\lambda)e^{-\delta_\lambda L}]e^{\delta_\lambda z}+[(1+\alpha_\lambda)e^{\delta_\lambda L}-\rho_\lambda(1-\alpha_\lambda)e^{\delta_\lambda L}]e^{-\delta_\lambda z}}{(1+\alpha_\lambda)^2e^{\delta_\lambda L}-(1-\alpha_\lambda)^2e^{-\delta_\lambda L}-\rho_\lambda(1-\alpha_\lambda^2)e^{\delta_\lambda L}+\rho_\lambda(1-\alpha_\lambda^2)e^{-\delta_\lambda L}} \tag{8}$$

where α_λ and δ_λ are expressed as (Pottier et al., 2005)

$$\alpha_\lambda=\sqrt{\frac{\overline{A}_{abs,\lambda}}{\overline{A}_{abs,\lambda}+2b_\lambda\overline{S}_{sca,\lambda}}} \quad\text{and}\quad \delta_\lambda=X\sqrt{\overline{A}_{abs,\lambda}(\overline{A}_{abs,\lambda}+2b_\lambda\overline{S}_{sca,\lambda})}. \tag{9}$$

Here, b_λ is the backward scattering fraction defined as

$$b_\lambda = \frac{1}{2}\int_{\pi/2}^{\pi} p_\lambda(0,\theta)\sin\theta\, d\theta. \quad (10)$$

Microalgae suspensions in PBRs scatter visible light strongly in the forward direction. Then, b_λ tends to zero, α_λ approaches unity, and $\delta_\lambda = \overline{A}_{abs,\lambda}X = \kappa_\lambda$. Thus, the above expression for $G_\lambda(z)$ can be simplified to (Lee et al., 2014)

$$G_\lambda(z) = q''_{in,\lambda} e^{-\overline{A}_{abs,\lambda}Xz} + \rho_\lambda q''_{in,\lambda} e^{-\overline{A}_{abs,\lambda}X(2L-z)}. \quad (11)$$

The first term represents the remainder of the incident irradiance after it has traveled a distance z in the microalgae suspension while the second term accounts for the incident irradiance that has traveled once through the suspension, got reflected by the back wall, and continued traveling a distance $(L-z)$ in the suspension. Note that reflectance $\rho_\lambda = 0$ for PBRs with a transparent back wall. This simplified expression has been validated against predictions by Eq. (8) and by the numerical solutions of the 3D RTE using the discontinuous Galerkin method combined with the discrete-ordinate method for outdoor open ponds and flat plate PBRs (Lee et al., 2014). Note that Eq. (11) differs from Beer-Lambert's law in that (i) it depends only on the absorption coefficient $\kappa_\lambda = \overline{A}_{abs,\lambda}X$ and not on the extinction coefficient $\beta_\lambda = (\overline{A}_{abs,\lambda} + \overline{S}_{sca,\lambda})X$ and (ii) it accounts for reflection within the PBR. More importantly, the simplified expression for the fluence rate $G_\lambda(z)$ given by Eq. (11) depends only on the average spectral mass absorption cross-section $\overline{A}_{abs,\lambda}$ of the suspension.

2.4. Growth kinetics and productivity

The time rate of change of the microorganism mass concentration $X(t)$ in continuous cultures satisfies the mass balance equation (Pires, 2015)

$$\frac{dX}{dt} = \langle\mu\rangle X - DX \quad (12)$$

where D (in h^{-1}) is the dilution rate of the culture and $\langle\mu\rangle$ (in h^{-1}) corresponds to the volume-average specific growth rate of the microorganisms. In addition, the volumetric biomass productivity $\langle r_X\rangle$ is defined as $\langle r_X\rangle = \langle\mu\rangle X$. For PBRs operated in continuous mode, steady-state conditions are achieved when $\frac{dX}{dt} = 0$. This condition is satisfied when $\langle\mu\rangle = D$ (Pires, 2015).

Several models have been developed to predict the average specific growth rate $\langle\mu\rangle$ as a function of the illumination conditions in the PBR over the PAR region. The most general approach is to define the average specific growth rate $\langle\mu\rangle$ over the entire flat-plate PBR depth L from the local growth rate $\mu(z)$ at location z according to (Fouchard et al., 2009)

$$\langle\mu\rangle = \frac{1}{L}\int_0^L \mu(z)\, dz. \quad (13)$$

The local growth rate $\mu(z)$ is related to the local oxygen production rate $J_{O_2}(z)$ (in $mol_{O_2}/kg_X \cdot s$) by Takache et al. (2012)

$$\mu(z) = \frac{J_{O_2}(z)M_x}{\nu_{O_2-X}}. \quad (14)$$

Here, M_x (in kg/mol) is the molar mass of the biomass and ν_{O_2-X} the stoichiometric coefficient of the oxygen production. Then, the local oxygen production rate $J_{O_2}(z)$ can be expressed as a function of the local rate of photon absorption (LRPA) $\mathcal{A}(z)$ according to (Takache et al., 2012)

$$J_{O_2}(z) = \rho_M \frac{K}{K+\mathcal{A}(z)}\phi'_{O_2}\mathcal{A}(z) - \frac{J_{NADH_2}}{\nu_{NADH_2-O_2}}\frac{K_r}{K_r+\mathcal{A}(z)} \quad (15)$$

where ρ_M is the maximum energy yield for photon conversion, ϕ'_{O_2} is the quantum yield of O_2 (in $mol_{O_2}/\mu mol_{h\nu}$) for the Z-scheme of photosynthesis, and K and K_r (in $\mu mol_{h\nu}/kg_X \cdot s$) are, respectively, the half-saturation constant for photosynthesis and the saturation constant describing the inhibition of respiration in light. Note that the first term on the right hand side of Eq. (15) represents oxygen production due to photosynthesis while the second term represents oxygen consumption due to respiration. Similarly, J_{NADH_2} and $\nu_{NADH_2-O_2}$ are the specific rate and stoichiometric coefficient of cofactor regeneration on the respiratory chain. The kinetic model presented by Eqs. (14) and (15) was developed and experimentally validated for the green microalgae *C. reinhardtii* by Takache et al. (2012). Recently, Pruvost and co-workers (Pruvost et al., 2016; Soulies et al., 2016) adjusted the model parameter values to adapt the model to *C. vulgaris* by fitting the model to experimentally measured biomass productivity at various culture dilution rates and incident irradiances. Detailed description of the kinetic model parameters as well as how they were estimated can be found in Cornet and Dussap (2009); Takache et al. (2012); Soulies et al. (2016). Table 1 summarizes the kinetic model parameters and their corresponding values for *C. vulgaris* (Soulies et al., 2016).

Finally, the LRPA $\mathcal{A}(z)$ can be expressed as (Cornet et al., 1992; Cornet and Dussap, 2009)

$$\mathcal{A}(z) = \int_{400}^{700} \overline{A}_{abs,\lambda} G_\lambda(z)\, d\lambda. \quad (16)$$

Similarly, the mean rate of photon absorption (MRPA) $\langle\mathcal{A}\rangle$ can be obtained by integrating the LRPA over the volume of the flat-plate PBR as

$$\langle\mathcal{A}\rangle = \frac{1}{L}\int_0^L \mathcal{A}(z)\, dz. \quad (17)$$

Here, it is interesting to note that, for strongly forward scattering media, the MRPA $\langle\mathcal{A}\rangle$ depends only on G_λ, $\overline{A}_{abs,\lambda}$, and L where $G_\lambda(z)$ is

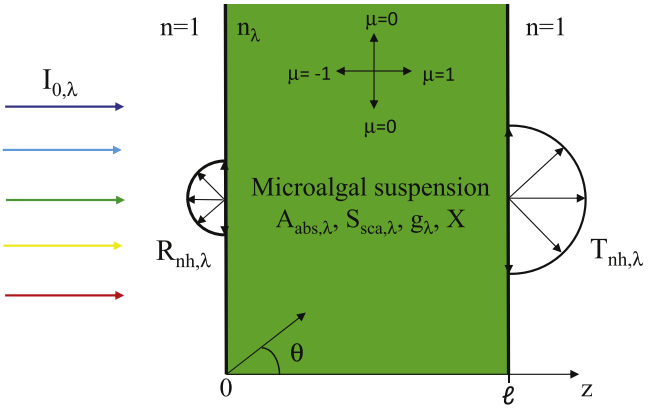

Fig. 1. Schematic of one-dimensional light transfer in a refracting, absorbing, and scattering microalgae suspension illuminated with collimated and normally incident light.

Table 1
Kinetic model parameters used for predicting biomass productivity of *C. vulgaris* (Soulies et al., 2016).

Parameter	Value	Units
M_x	0.024	kg/mol
J_{NADH_2}	1.80×10^{-3}	mol_{NADH_2}/kg s
ν_{O_2-X}	1.13	mol_{O_2}/mol_X
ρ_M	0.8	
ϕ'_{O_2}	1.10×10^{-7}	$mol_{O_2}/\mu mol_{h\nu}$
$\nu_{NADH_2-O_2}$	2	mol_{NADH_2}/mol_{O_2}
K	4.0×10^4	$\mu mol_{h\nu}$/kg s
K_r	500	$\mu mol_{h\nu}$/kg s

given by Eq. (11). This emphasizes the importance of determining the spectral mass absorption cross-section $\overline{A}_{abs,\lambda}$ over the PAR region.

2.5. Microalgae radiation characteristics

The radiation characteristics of microalgae can be directly measured experimentally (Berberoğlu and Pilon, 2007; Berberoğlu et al., 2008; Pilon et al., 2011) or predicted theoretically (Pottier et al., 2005; Berberoğlu et al., 2007; Dauchet et al., 2015). Direct experimental measurements can be performed on microorganisms of any size and shape. However, they require expensive equipment and can be time consuming, and need to be repeated for different growth conditions, such as different pH, temperature, and/or photon flux density change, as these parameters can alter the radiation characteristics of the microalgae (Berberoğlu et al., 2008; Pilon et al., 2011). Recently, Bellini et al. (2014) developed an experimental method to determine the absorption $\overline{A}_{abs,\lambda}$ and the transport scattering $(1-g_\lambda)\overline{S}_{sca,\lambda}$ cross-sections of microalgae. The authors measured the total reflectance (diffuse plus specular reflectance) and the normal–hemispherical transmittance of microalgae suspensions using a double integrating sphere spectrophotometer and retrieved $\overline{A}_{abs,\lambda}$ and $(1-g)\overline{S}_{sca,\lambda}$ using the inverse-adding-doubling (IAD) method (Prahl et al., 1993). The microalgae suspensions featured a concentration between 1.1×10^{13} and 2.4×10^{13} cells/m^3. This method was not able to estimate the absorption and the transport scattering cross-section accurately especially for samples with low absorption coefficient. Indeed, the authors stated that "in samples with low absorption and high scattering coefficients, the unwanted light losses may be interpreted by the IAD algorithm as absorption phenomena inside the sample rather than losses in the outside world, leading to an overestimation of the absorption coefficient" (Bellini et al., 2014). They recommended for this method to be only used for qualitative analysis of microalgae cultures. Alternatively, the radiation characteristics of microalgae can be estimated theoretically using electromagnetic wave theory and solutions of Maxwell's equations such as the Lorenz–Mie theory. However, such theoretical predictions rely on several simplifying assumptions such as treating the cells as homogeneous and spherical with some effective spectral complex index of refraction predicted based on simplified models (Pottier et al., 2005; Berberoğlu et al., 2007; Dauchet et al., 2015). For example, fractal colonies and aggregates of microalgae (Kandilian et al., 2015) and filamentous cyanobacteria such as *Nostoc pondiforme* and *Anabaena iyengari* (Lee and Pilon, 2013), or the dumbbell shaped cyanobacteria *Synechocystis* sp. (Heng et al., 2015) cannot be treated as spherical. By contrast, a simple experimental method that is able to determine the absorption cross-section of microorganisms with any arbitrary shapes and optical properties could be valuable.

This paper presents a simple method for measuring the spectral absorption cross-section $\overline{C}_{abs,\lambda}$ or $\overline{A}_{abs,\lambda}$ from simple and rapid measurements of normal–hemispherical transmittance and reflectance of relatively concentrated suspensions in conventional cuvettes. In fact, we have argued that the absorption cross-section is sufficient to predict the local fluence rate $G_\lambda(z)$, the MRPA $\langle A\rangle$, and the average growth rate $\langle\mu\rangle$.

3. Materials and methods

3.1. Microalgae cultivation and sample preparation

The microalgae *C. vulgaris* CCAP 211/19 were obtained from the culture collection of algae and protozoa (CCAP, Scotland, UK). The microorganisms were cultivated in a 4 cm thick, 1.4 L torus PBR constructed with transparent PMMA described in detail in Pottier et al. (2005). The PBR was illuminated with 200 $\mu mol_{h\nu}/m^2$ s white LEDs incident on one side. It was operated in continuous mode by injection of fresh medium at the dilution rate D of 0.06 h^{-1} using a peristaltic pump. The microalgae were grown in modified Sueoka medium with the following composition (in grams per liter of MilliQ water): NH_4Cl 1.45, $MgSO_4$–$7H_2O$ 0.28, $CaCl_2$ 0.05, KH_2PO_4 0.61, $NaHCO_3$ 1.68, $ZnSO_4$–$7H_2O$ 0.022, H_3BO_3 0.0114, $MnCl_2$–$4H_2O$ 0.00506, $CoCl_2$–$6H_2O$ 0.00161, $CuSO_4$–$5H_2O$ 0.00157, $FeSO_4$–$7H_2O$ 0.00499, $(NH_4)_6Mo_7O_{24}$–$4H_2O$ 0.0011, KOH 0.05, Na_2EDTA 0.02. The culture temperature was maintained at 22 °C thanks to a liquid cooled heat exchanger attached to the stainless steel PBR back wall. The culture medium pH was continuously monitored using a pH sensor (Mettler Toledo SG 3253) and was maintained at 7.5 by automatically injecting CO_2 gas when it exceeded 7.5. Agitation of the culture was achieved by mechanically mixing the culture using a marine propeller attached to an electric motor. The culture under steady-state continuous operation had dry biomass concentration X of 0.33 g/L. To obtain samples with larger biomass concentrations, a small volume of culture was harvested and centrifuged at 10,000 g (ThermoScientific Sorvall RC 6 Plus, Massachusetts, USA) for 5 min at 4 °C and suspended in 3 ml of phosphate buffer saline (PBS) solution. The volume of culture sampled was chosen based on the biomass concentration desired for optical measurements and ranged from 0.035 to 111 g/L. Note that the biomass concentration of only the most concentrated sample was measured, i.e., 111 ± 5 g/L and the biomass concentrations of the remaining samples, namely, 55.6 ± 2.5, 11.1 ± 0.5, 5.56 ± 0.25, 1.11 ± 0.05, 0.556 ± 0.025, and 0.111 ± 0.0125 g/L, were estimated based on the dilution performed.

3.2. Culture characterization

The cell size distribution of *C. vulgaris* was measured using 165 microscope images captured using a digital camera (AxioCam MRc) mounted on an optical microscope (Zeiss Axio Scope A1). The diameters of 2873 cells were measured manually using an image processing software (Axio Vision Routine) and their volume equivalent sphere radius was reported for the sake of completeness. These results were not used in either experimental approaches investigated.

The culture dry biomass concentration X (in g/L) was determined gravimetrically by filtering 5 mL of culture through a pre-dried and pre-weighed 0.45 μm pore size glass-fiber filter (Whatman GF/F). The filters were dried overnight in an oven at 105 °C and weighed, in an analytical balance (Mettler Toledo XA204, Columbus, OH) with a sensitivity of 0.1 mg, after being cooled in a desiccator for 10 min. The samples were analyzed in triplicates and the reported biomass concentration corresponded to the mean value. In addition, the cell density N_T (in #/m^3) was counted using a 200 μm deep Malassez counting chamber.

The volume fraction of water in the cells x_w was estimated using the relation derived by Pottier et al. (2005) and given by

$$x_w = 1-\frac{X}{N_T}\frac{1}{V_{32}\rho_{dm}} \tag{18}$$

where ρ_{dm} corresponds to the density of dry biomass and was taken as 1350 kg/m^3 (Dauchet, 2012) while V_{32} is the cell volume corresponding to the Sauter mean diameter of the microorganisms. The latter is defined as the diameter of a sphere that has the same volume to surface area ratio as the original cell.

The concentration of photosynthetic pigments in *C. vulgaris* grown under the above mentioned conditions were estimated spectrometrically in terms of mass of pigments per unit volume of suspension (mg/m^3). A volume of 0.5 mL of culture was first centrifuged at 13,400 rpm (12,100 g) for 10 min. The medium was discarded and the cells were resuspended in 1.25 mL pure methanol and sonicated for 10 s. Pigments were extracted for 1 h at 45°C and

the extract was centrifuged. The optical density OD_λ of the supernatant was measured at wavelengths 750, 665, 652, and 480 nm using a UV-VIS-NIR spectrophotometer (Agilent Cary 5000, Santa Clara, CA). All extractions were performed in triplicates. Chlorophyll *a* and *b* concentrations, respectively denoted by C_{Chla} and C_{Chlb} (in mg/L), were estimated according to the correlations (Ritchie, 2006)

$$C_{Chla} = [-8.0962(OD_{652} - OD_{750}) + 16.5169(OD_{665} - OD_{750})]V_2\ell^{-1}V_1^{-1} \quad (19)$$

and $$C_{Chlb} = [27.4405(OD_{652} - OD_{750}) - 12.1688(OD_{665} - OD_{750})]V_2\ell^{-1}V_1^{-1} \quad (20)$$

where V_1 and V_2 are the volumes of the culture and of the solvent (methanol), respectively while ℓ is the thickness of the cuvette used to measure the optical density. Similarly, the total photoprotective (PPC) and photosynthetic (PSC) carotenoid concentration $C_{PPC+PSC}$ (in mg/L) was estimated according to (Strickland and Parsons, 1968)

$$C_{PPC+PSC} = 4(OD_{480} - OD_{750})V_2\ell^{-1}V_1^{-1}. \quad (21)$$

The corresponding mass fraction of pigment "*i*" per dry weight of biomass can be estimated as $w_i = C_i/X$.

3.3. Direct radiation characteristics measurements

3.3.1. Experiments

First, the total scattering phase function $p(\mu_0)$ of the microalgae suspension was measured at 632.8 nm using a polar nephelometer equipped with He–Ne laser. The experimental setup and data analysis were previously reported in detail by Berberoğlu et al. (2008) and need not be repeated. Due to probe interference with the incident laser beam, it was only possible to collect measurements for scattering angles θ_0 up to 160°. Then, the asymmetry factor g_{633} and the back-scattered fraction b_{633} at 632.8 nm were estimated according to Eqs. (3) and (10), respectively.

Second, the normal–normal transmittance of dilute suspensions of *C. vulgaris* in a cuvette, denoted by $T_{nn,\lambda}$, was measured using a UV-VIS-NIR spectrophotometer equipped with a detector with a 8° half acceptance angle Θ_a (Agilent Cary 5000, Santa Clara, CA). The normal–hemispherical transmittances $T_{nh,\lambda}$ of the same suspensions were measured using an integrating sphere attachment (Agilent Cary DRA-2500, Santa Clara, CA) to the spectrophotometer. Due to masking by the cuvette holder, the cuvette area exposed to the normally incident beam was 20 × 8 mm and the cuvette holder was positioned directly in front of the 19 × 17 mm opening of the integrating sphere. The size of the incident beam was 9 × 5 mm. These measurements were performed with 1 cm pathlength quartz cuvettes (11010-40 Hellma Analytics, Mülheim, Germany) in the wavelength range from 350 to 750 nm with 1 nm spectral resolution. To avoid absorption and scattering by the growth medium, the microalgae were centrifuged at 13,400 rpm for 10 min and washed twice with PBS solution and suspended in PBS. Two biomass concentrations were considered, namely 0.035 and 0.049 dry mass g/L. Such dilute suspensions ensure that single scattering prevails so that measurements of $T_{nn,\lambda}$ and $T_{nh,\lambda}$ can be used in the direct measurements of the radiation cross-sections of *C. vulgaris*. Note that the samples were manually shaken prior to each of the transmission measurements so as to prevent sedimentation. The sample normal–normal $T_{nn,\lambda}$ and normal–hemispherical $T_{nh,\lambda}$ transmittances were measured three times and the results were averaged for each concentration.

3.3.2. Data analysis

The extinction coefficient of the microalgae suspension β_λ was obtained from normal–normal transmittance measurements. In order to correct for the effects of reflection and refraction by the cuvette, the measurements were calibrated using the transmittance of the reference medium (e.g., PBS) denoted by $T_{nn,\lambda,ref}$. Then, the apparent extinction coefficient β^*_λ was defined as (Davies-Colley et al., 1986)

$$\beta^*_\lambda = -\frac{1}{\ell}\ln\left(\frac{T_{nn,\lambda}}{T_{nn,\lambda,ref}}\right). \quad (22)$$

In addition, microalgae are relatively large compared with the wavelength of light and thus scatter strongly in the forward direction. A fraction ϵ_n of the light that is scattered in the forward direction reaches the detector due to its finite acceptance angle. This fraction can be expressed as a function of the scattering phase function $p_\lambda(\theta)$ previously measured (Agrawal and Mengüç, 1991; Privoznik et al., 1978)

$$\epsilon_n = \frac{1}{2}\int_0^{\Theta_a} p_\lambda(\theta)\sin\,\theta\,d\theta \quad (23)$$

where Θ_a is the half acceptance angle of the detector. Then, the apparent extinction coefficient can be related to the actual absorption and scattering coefficients by (Davies-Colley et al., 1986),

$$\beta^*_\lambda = \kappa_\lambda + \sigma_{s,\lambda} - \epsilon_n\sigma_{s,\lambda} \quad \text{so that} \quad \beta_\lambda = \frac{\beta^*_\lambda - \epsilon_n\kappa_\lambda}{1-\epsilon_n}. \quad (24)$$

The absorption coefficient κ_λ was obtained from normal–hemispherical transmittance $T_{nh,\lambda}$ measurements. Then, the apparent absorption coefficient κ^*_λ can be expressed as

$$\kappa^*_\lambda = -\frac{1}{\ell}\ln\left(\frac{T_{nh,\lambda}}{T_{nh,\lambda,ref}}\right). \quad (25)$$

Due to imperfect reflections at the inner surface of the integrating sphere and to the geometry of the experimental setup, the detector was unable to capture all the scattered light. To account for these phenomena, the apparent absorption coefficient κ^*_λ can be related to the absorption and scattering coefficients by (Pilon et al., 2011)

$$\kappa^*_\lambda = \kappa_\lambda + (1-\epsilon_h)\sigma_{s,\lambda} \quad (26)$$

where ϵ_h represents the fraction of scattered light not collected by the integrating sphere or not measured by the detector. It accounts for backward scattered light that does not enter the integrating sphere and for forward scattered light that does not reach the detector because of imperfect reflection, for example. This correction factor is assumed to be constant over the PAR region. Davies-Colley et al. (1986) assumed that the microalgae did not absorb radiation at wavelength λ_o. For example, λ_o=750 nm for *Chlamydomonas reinhardtii* (Berberoğlu et al., 2008) and *Chlorella sp.* (Berberoğlu et al., 2009). At this wavelength, the absorption coefficient vanishes, i.e., $\kappa_\lambda = 0\ \mathrm{m}^{-1}$, and ϵ_h can be estimated from Eq. (26) as (Pilon et al., 2011)

$$\epsilon_h = 1 - \frac{\kappa^*_{\lambda_o}}{\sigma_{s,\lambda_o}} \quad (27)$$

Combining Eqs. (24)–(27) yields the expression for the actual absorption coefficient κ_λ given, in terms of measurable quantities, by (Pilon et al., 2011)

$$\kappa_\lambda = \kappa^*_\lambda - \kappa^*_{\lambda_o}\left(\frac{\beta^*_\lambda - \kappa^*_\lambda}{\beta^*_{\lambda_o} - \kappa^*_{\lambda_o}}\right) \quad (28)$$

Finally, the actual extinction coefficient β_λ can be obtained by substituting κ_λ into Eq. (24). Then, the scattering coefficient can be computed using the definition $\sigma_{s,\lambda} = \beta_\lambda - \kappa_\lambda$.

The absorption and scattering coefficients κ_λ and $\sigma_{s,\lambda}$ were divided by the sample dry biomass concentration *X* to obtain the average spectral mass absorption and scattering cross-sections $\overline{A}_{abs,\lambda}$ and $\overline{S}_{sca,\lambda}$ according to Eq. (6). The spectral cross-sections $\overline{A}_{abs,\lambda}$ and $\overline{S}_{sca,\lambda}$ for different cell densities/concentrations should collapse onto a single line if single and independent scattering

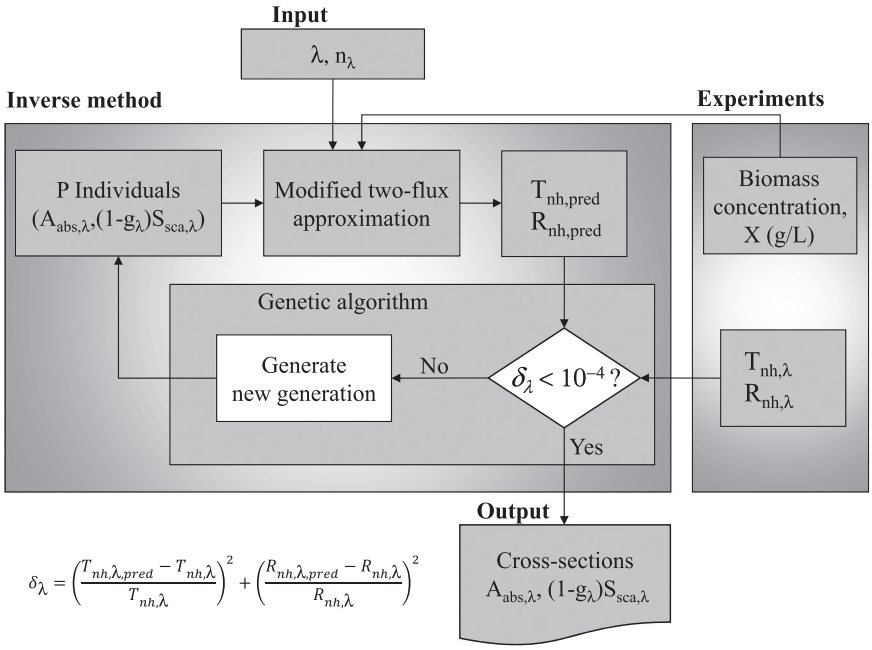

Fig. 2. Block diagram of the procedure used to retrieve the average mass absorption and transport scattering cross-sections $\overline{A}_{abs,\lambda}$ and $(1-g_\lambda)\overline{S}_{sca,\lambda}$ of concentrated suspensions at a given wavelength λ from spectral normal–hemispherical transmittance and reflectance measurements. We used $P=120$ individuals per generation for a maximum of 50 generations.

prevailed (Van De Hulst, 1957). This provided further validation of the experimental procedure and data analysis.

Finally, the direct measurement method with the previously described apparatus and data analysis were successfully validated by comparing the measurements with predictions by Lorenz–Mie theory for monodisperse spherical latex particles 1.98 ± 0.01 or 4.518 ± 0.158 μm in diameter (Polysciences Inc., Warrington, PA).

4. Inverse method

4.1. Experiments

The normal–hemispherical transmittance $T_{nh,\lambda}$ and reflectance $R_{nh,\lambda}$ of *C. vulgaris* suspensions, with mass concentration ranging from 0.111 g/L to 111 g/L, were systematically measured using the above described spectrophotometer/integrating sphere assembly. Measurements for the different concentrations were performed within less than 1 h in order to minimize changes in cell biomass, composition, and pigment concentrations and thus their radiation characteristics during the successive measurements. For the relatively large concentrations considered, multiple scattering prevailed and the direct measurement method, previously described in Section 3.3 and valid for single scattering, could not be used. Instead, experimentally measured values of $T_{nh,\lambda}$ and $R_{nh,\lambda}$ were used as input parameters in the inverse method to retrieve the average spectral mass absorption $\overline{A}_{abs,\lambda}$ and scattering $\overline{S}_{sca,\lambda}$ cross-sections of *C. vulgaris*.

4.2. Forward problem formulation

Let us consider one-dimensional radiation transfer in microalgal suspension exposed to normally incident, collimated, monochromatic, and randomly polarized light as illustrated in Fig. 1. The suspension was assumed to be well-mixed and the microorganisms were randomly oriented and azimuthally symmetric. Under these conditions and due to strong forward scattering by microalgae suspensions and the relatively thin cuvettes, light transfer can be

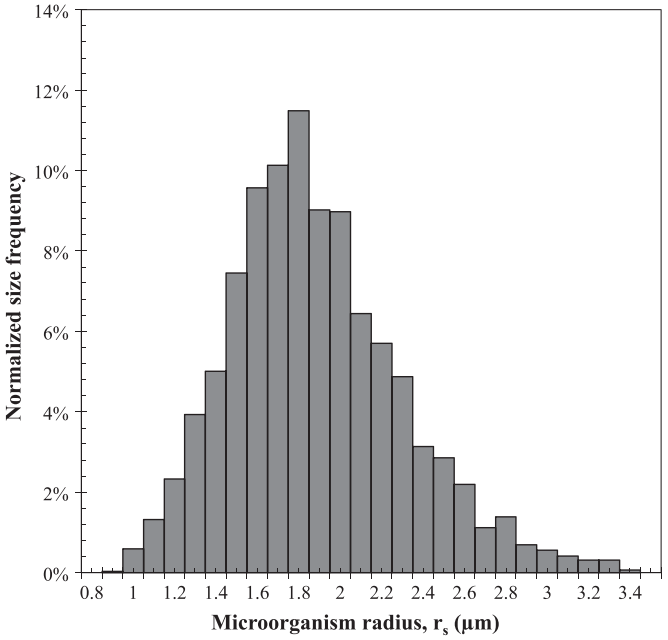

Fig. 3. Experimentally measured size distribution of *C. vulgaris* with mean radius $\overline{r} = 1.98$ μm.

assumed to be one-dimensional (Pilon et al., 2011; Pottier et al., 2005; Lee et al., 2014; Dauchet et al., 2015; Stramski and Piskozub, 2003). We further assumed that the scattering phase function was given by the transport approximation. Then, the spectral normal–hemispherical transmittance and reflectance of the suspension, after accounting for internal reflection, can be expressed as (Dombrovsky et al., 2005)

$$T_{nh,\lambda,pred} = T^0_{nh,\lambda} + \frac{D_\lambda}{2}\left[(1+\rho_{1,\lambda})\exp\left(-\tau_{tr,\lambda,\ell}\right) + A_\lambda/\zeta_\lambda\right] \tag{29}$$

and

$$R_{nh,\lambda,pred} = R^0_{nh,\lambda} + \frac{D_\lambda}{2}\left(1 + B_\lambda/\zeta_\lambda + C_{tr,\lambda}\right) \tag{30}$$

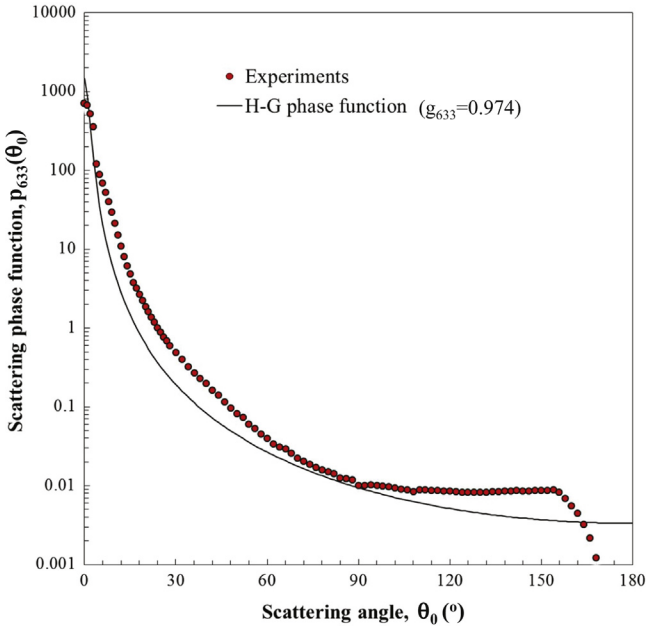

Fig. 4. Experimentally measured phase function of *C. vulgaris* at 632.8 nm along with the associated Henyey–Greenstein phase function for asymmetry factor $g_{633}=0.974$.

where $\tau_{tr,\lambda,\ell}$ is the transport optical thickness defined as $\tau_{tr,\lambda,\ell}=\beta_{tr,\lambda}\ell=[\overline{A}_{abs,\lambda}+(1-g_\lambda)\overline{S}_{sca,\lambda}]X\ell$. Here, $R^0_{nh,\lambda}$ and $T^0_{nh,\lambda}$ are the spectral normal–hemispherical reflectance and transmittance of the suspension ignoring multiple scattering expressed as (Dombrovsky et al., 2005; Modest, 2013)

$$R^0_{nh,\lambda}=\frac{\rho_{1,\lambda}+(1-\rho_{1,\lambda})^2C_{tr,\lambda}}{1-\rho_{1,\lambda}C_{tr,\lambda}} \quad \text{and} \quad T^0_{nh,\lambda}=\frac{(1-\rho_{1,\lambda})^2}{1-\rho_{1,\lambda}C_{tr,\lambda}}\exp(-\tau_{tr,\lambda,\ell}) \tag{31}$$

where $\rho_{1,\lambda}$ is the normal–normal reflectivity of the quartz/air interface given by Fresnel's equations. For an optically smooth surface with normally incident radiation and assuming that the absorption index k_λ of the quartz was negligible compared with its refractive index n_λ so that

$$\rho_{1,\lambda}=\frac{(n_\lambda-1)^2}{(n_\lambda+1)^2} \tag{32}$$

The parameters A_λ, B_λ, $C_{tr,\lambda}$, and D_λ are defined as (Dombrovsky et al., 2005)

$$A_\lambda=\frac{(\gamma_{1,\lambda}-\gamma_{2,\lambda}\rho_{1,\lambda})(\varphi_\lambda s_\lambda+c_\lambda)\exp(-\tau_{tr,\lambda,L})-(\gamma_{2,\lambda}-\gamma_{1,\lambda}C_{tr,\lambda})}{(1+\varphi_\lambda^2)s_\lambda+2\varphi_\lambda c_\lambda} \tag{33}$$

$$B_\lambda=\frac{(\gamma_{1,\lambda}-\gamma_{2,\lambda}\rho_{1,\lambda})\exp(-\tau_{tr,L})-(\gamma_{2,\lambda}-\gamma_{1,\lambda}C_{tr,\lambda})(\varphi_\lambda s_\lambda+c_\lambda)}{(1+\varphi_\lambda^2)s_\lambda+2\varphi_\lambda c_\lambda} \tag{34}$$

$$C_{tr,\lambda}=\rho_{1,\lambda}\exp(-2\tau_{tr,\lambda,\ell}) \tag{35}$$

$$D_\lambda=\frac{\gamma_\lambda(1-\mu_{c,\lambda}^2)\chi_\lambda\zeta_\lambda^2}{\zeta_\lambda^2-1} \tag{36}$$

Here, the parameters γ_λ, $\mu_{c,\lambda}$, $\overline{\gamma}_\lambda$, $\gamma_{1,\lambda}$, $\gamma_{2,\lambda}$, φ_λ, ζ_λ, s_λ, and c_λ are given by Dombrovsky et al. (2005)

$$\gamma_\lambda=\frac{1-\rho_{1,\lambda}}{1+\rho_{1,\lambda}},\ \mu_{c,\lambda}=\frac{(n_\lambda^2-1)^{1/2}}{n_\lambda},$$

$$\overline{\gamma}_\lambda=\frac{\gamma_\lambda}{1+\mu_{c,\lambda}},\ \gamma_{1,\lambda}=1-2\overline{\gamma}_\lambda,\gamma_{2,\lambda}=1+2\overline{\gamma}_\lambda,$$

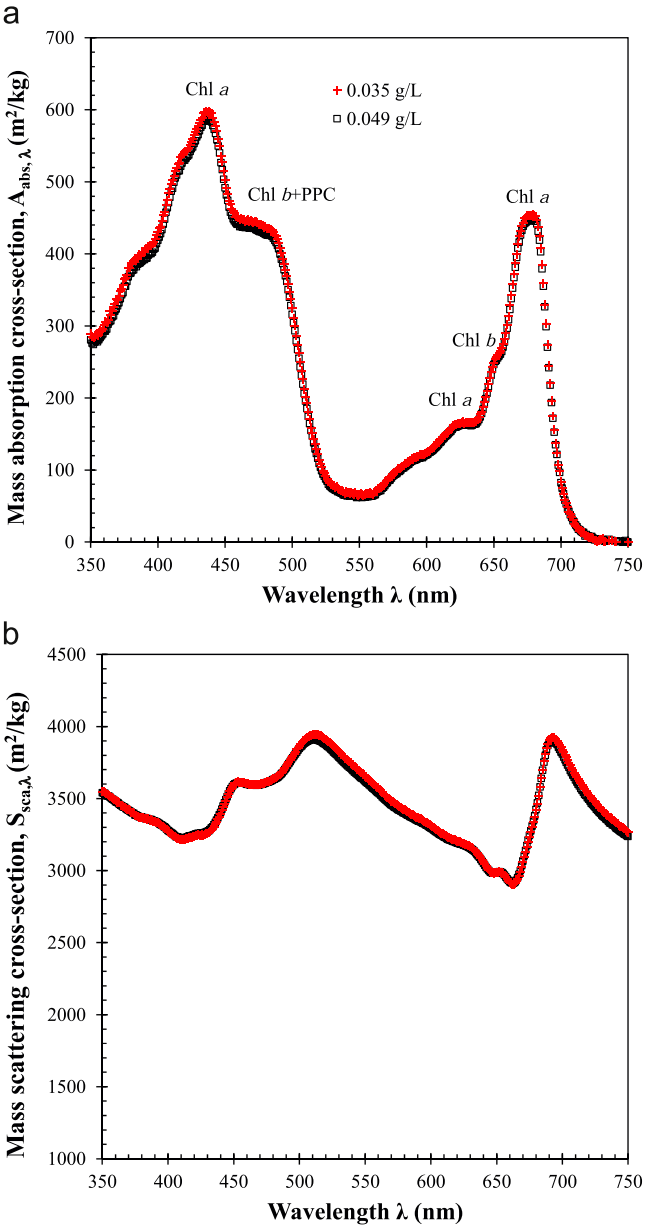

Fig. 5. Directly measured average spectral mass absorption $\overline{A}_{abs,\lambda}$ and scattering $\overline{S}_{sca,\lambda}$ cross-sections of *C. vulgaris* suspensions between 350 and 750 nm for biomass concentrations X of 0.035 and 0.049 g/L.

$$\chi_\lambda=\frac{\omega_{tr,\lambda}}{1-\omega_{tr,\lambda}}\frac{1-\rho_{1,\lambda}}{1-\rho_{1,\lambda}C_{tr,\lambda}},\ \varphi_\lambda=2\overline{\gamma}_\lambda/\zeta_\lambda,\ \zeta_\lambda^2=\frac{4}{(1+\mu_{c,\lambda})^2}\frac{1-\omega_{tr,\lambda}}{1-\omega_{tr,\lambda}\mu_{c,\lambda}},$$

$$s_\lambda=\sinh(\zeta_\lambda\tau_{tr,\lambda,\ell}), \quad \text{and} \quad c_\lambda=\cosh(\zeta_\lambda\tau_{tr,\lambda,\ell}) \tag{37}$$

where $\mu_{c,\lambda}$ is the director cosine of the critical angle θ_c beyond which total internal reflection occurs while the transport single scattering albedo is defined as $\omega_{tr,\lambda}=\sigma_{tr,s,\lambda}/\beta_{tr,\lambda}$. In order to predict the normal–hemispherical transmittance and reflectance $T_{nh,\lambda}$ and $R_{nh,\lambda}$ using Eqs. (29)–(37), one needs to know (i) the thickness ℓ of the suspension, (ii) the index of refraction of the quartz cuvette n_λ, (iii) the absorption coefficient of the suspension κ_λ, and (iv) the transport scattering coefficient $\sigma_{s,tr,\lambda}=\sigma_{s,\lambda}(1-g_\lambda)$. Here, the thickness ℓ of the cuvette was 10 mm. The spectral refraction index n_λ of quartz was given by the dispersion relation (Heraeus, 2015)

$$n_\lambda^2-1=\frac{B_1\lambda^2}{\lambda^2-C_1}+\frac{B_2\lambda^2}{\lambda^2-C_2}+\frac{B_3\lambda^2}{\lambda^2-C_3} \tag{38}$$

where the wavelength λ is expressed in μm and ranges from 0.2 to 2.5 μm. The constants B_1, B_2, B_3, C_1, C_2, and C_3 are respectively equal to $4.73115591 \times 10^{-1}$, $6.31038719 \times 10^{-1}$, $9.06404498 \times 10^{-1}$, $1.29957170 \times 10^{-2}\ \mu m^2$, $4.12809220 \times 10^{-3}\ \mu m^2$, and $9.87685322 \times 10^{1}\ \mu m^2$ (Heraeus, 2015). On the other hand, in the visible part of the spectrum, quartz can be treated as non-absorbing, i.e., $k_\lambda \approx 0$ (Heraeus, 2015). This corresponded to μ_c around 0.73 or to a critical angle θ_c, for total internal reflection, of about 43° while the reflectivity $\rho_{1,\lambda}$ was about 3.5%.

4.3. Inverse method optimization

Fig. 2 shows a block diagram of the procedure used to simultaneously retrieve the spectral mass absorption $\overline{A}_{abs,\lambda}$ and transport scattering $(1-g_\lambda)\overline{S}_{sca,\lambda}$ cross-sections from the normal–hemispherical transmittance $T_{nh,\lambda}$ and reflectance $R_{nh,\lambda}$ measurements over the PAR region. The objective is to find the values of $\overline{A}_{abs,\lambda}$ and $(1-g_\lambda)\overline{S}_{sca,\lambda}$ that minimize the difference between the predicted and experimentally measured normal–hemispherical transmittance and reflectance of the microalgal suspension in the least-square sense. Various optimization algorithms can be used to minimize, for each wavelength, the objective function δ_λ defined as,

$$\delta_\lambda = \left(\frac{T_{nh,\lambda,pred} - T_{nh,\lambda}}{T_{nh,\lambda}}\right)^2 + \left(\frac{R_{nh,\lambda,pred} - R_{nh,\lambda}}{R_{nh,\lambda}}\right)^2. \quad (39)$$

Here, the inverse method to retrieve $\overline{A}_{abs,\lambda}$ and $(1-g_\lambda)\overline{S}_{sca,\lambda}$ was implemented in Microsoft Excel using the built in non-linear optimization solver based on the generalized reduced gradient (GRG) algorithm. A simple Excel file with instruction is available in digital form online (Pilon, 2015) or directly from the corresponding author upon request. For the sake of comparison, the inverse method was also implemented based on genetic algorithm using the general purpose function optimization code PIKAIA (Charbonneau and Knapp, 1995; Charbonneau, 2002, 2002). Here, the spectral mass absorption and transport scattering cross-sections $\overline{A}_{abs,\lambda}$ and $(1-g_\lambda)\overline{S}_{sca,\lambda}$ were retrieved and assumed to range from 0 to 1000 m^2/kg based on past experience and on the literature (Pilon et al., 2011). The genetic algorithm used a maximum of 50 generations with a population consisting of $P=120$ individuals. The convergence criteria was set as $\delta_\lambda < 10^{-4}$. Note that both retrieval methods gave identical results.

5. Results and discussion

5.1. Chlorella vulgaris characterization

Fig. 3 shows the measured size distribution of *C. vulgaris* obtained with 2873 cells. The cells featured a mean radius $\overline{r}_s$ of 1.98 μm with a standard deviation of 0.41 μm. Moreover, the mean ratio of minimum and maximum axis of each cell fitted to an ellipse was 0.81. The cell number density N_T was related to the dry biomass concentration X by $N_T = 1.17 \times 10^{14}X$. Thus, the mass fraction of water in the microorganisms was estimated as $x_w=82$ wt.% based on Eq. (18). The pigment concentrations were measured spectrophotometrically according to the procedure described earlier. The concentrations of Chl *a*, Chl *b*, and total carotenoids were such that $C_{Chla} = 25.95 \pm 0.82$ mg/L, $C_{Chlb} = 4.81 \pm 0.36$ mg/L, $C_{PPC+PSC} = 6.14 \pm 0.29$ mg/L. These results corresponded to the weight percentage $w_{Chla} = 4.41 \pm 0.14$ wt.%, $w_{Chlb} = 0.82 \pm 0.05$ wt.%, and $w_{PPC+PSC} = 1.04 \pm 0.06$ wt.%.

5.2. Direct measurements

Fig. 4 shows the azimuthally symmetric scattering phase function of *C. vulgaris* measured experimentally at 632.8 nm. It is evident that *C. vulgaris* scattered visible light strongly in the forward direction, as expected for such large scatterers with mean size parameter $\overline{\chi} = 2\pi\overline{r}_s/\lambda$ ranging from 16 to 36 over the PAR. In fact, the asymmetry factor g_{633} and back-scattered fraction b_{633} were 0.974 and 0.0042, respectively. Fig. 4 also plots the corresponding Henyey–Greenstein approximate phase function. In addition, the fraction ϵ_n of light scattered in the forward direction reaching the detector was estimated to be $\epsilon_n = 0.71$. This value was used in the direct measurements of the extinction cross-section [Eq. (24)].

Fig. 5a and b respectively plot the average mass absorption $\overline{A}_{abs,\lambda}$ and scattering $\overline{S}_{sca,\lambda}$ cross-sections (in m^2/kg) as functions of wavelength between 350 and 750 nm measured directly for small biomass concentrations of 0.035 and 0.049 g/L. First, the cross-sections measured for both concentrations collapse on the same curve confirming that single scattering conditions prevailed

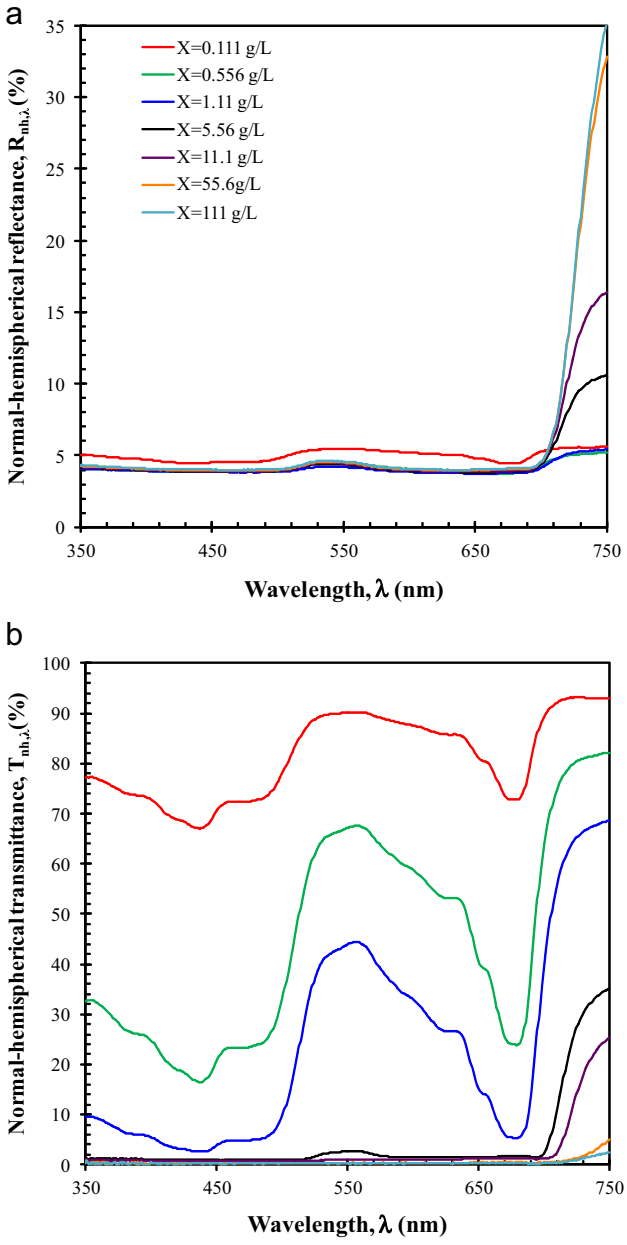

Fig. 6. Experimentally measured normal–hemispherical (a) reflectance $R_{nh,\lambda}$ and (b) transmittance $T_{nh,\lambda}$ between 350 and 750 nm for *C. vulgaris* suspensions in quartz cuvettes with a path length of 1 cm with different values of biomass concentrations X ranging from 0.111 to 111 g/L.

(Van De Hulst, 1957). Fig. 5 also indicates that the scattering cross-section $\overline{S}_{sca,\lambda}$ was much larger than the absorption cross-section $\overline{A}_{abs,\lambda}$. Note, however, that the transport scattering cross-section $\overline{S}_{sca,\lambda}(1-g_\lambda)$ was smaller than the absorption cross-section since g_λ approached unity. The absorption peaks of Chl *a* were apparent at 435, 630, and 676 nm, based on the absorption peaks of *in vivo* photosynthetic pigments reported by Bidigare et al. (1990). The shoulder from 455 to 485 nm can be attributed to superposition of the absorption peaks of Chl *b* at 475 nm and of PPC around 462 and 490 nm (Bidigare et al., 1990). Another absorption peak of Chl *b* can be observed around 650 nm. These absorption and scattering cross-sections obtained from direct measurements will be treated as references in evaluating the performance of the inverse method.

5.3. Results from inverse method

5.3.1. Normal–hemispherical transmittance and reflectance

Fig. 6a and b respectively show the normal–hemispherical reflectance $R_{nh,\lambda}$ and transmittance $T_{nh,\lambda}$ as a function of wavelength between 350 and 750 nm for *C. vulgaris* concentration ranging from 0.111 to 111 g/L. It indicates that the transmittance decreased sharply as the mass concentration increased. In fact, for concentration larger or equal to 5.56 g/L, the transmittance, over the PAR region, fell below the detection limit of the spectrophotometer. On the other hand, the reflectance remained relatively constant around 4%. Interestingly, it increased with increasing concentration beyond 700 nm due to the fact that the suspension absorption coefficient vanished and scattering, including back-scattering, increased. Overall, only normal–hemispherical transmittance and reflectance measurements for cell concentrations 0.111, 0.556, and 1.11 g/L had a large enough signal to noise ratio to be used in the inverse method. Data for larger concentrations led to very noisy and unrealistic retrieved values of both $\overline{A}_{abs,\lambda}$ and $\overline{S}_{sca,\lambda}(1-g_\lambda)$.

5.3.2. Model validation

The measured transmittance $T_{nh,\lambda}$ and reflectance $R_{nh,\lambda}$ of *C. vulgaris* suspensions of biomass concentration X equal to 0.111, 0.556, and 1.11 g/L over the PAR region were in reasonably good agreement with predictions by the modified two-flux approximation (Eqs. (29)–(37)) using the average absorption $\overline{A}_{abs,\lambda}$ and scattering $\overline{S}_{sca,\lambda}$ cross-sections and the asymmetry factor g measured directly with dilute suspensions (see Supplementary Material). This establishes that

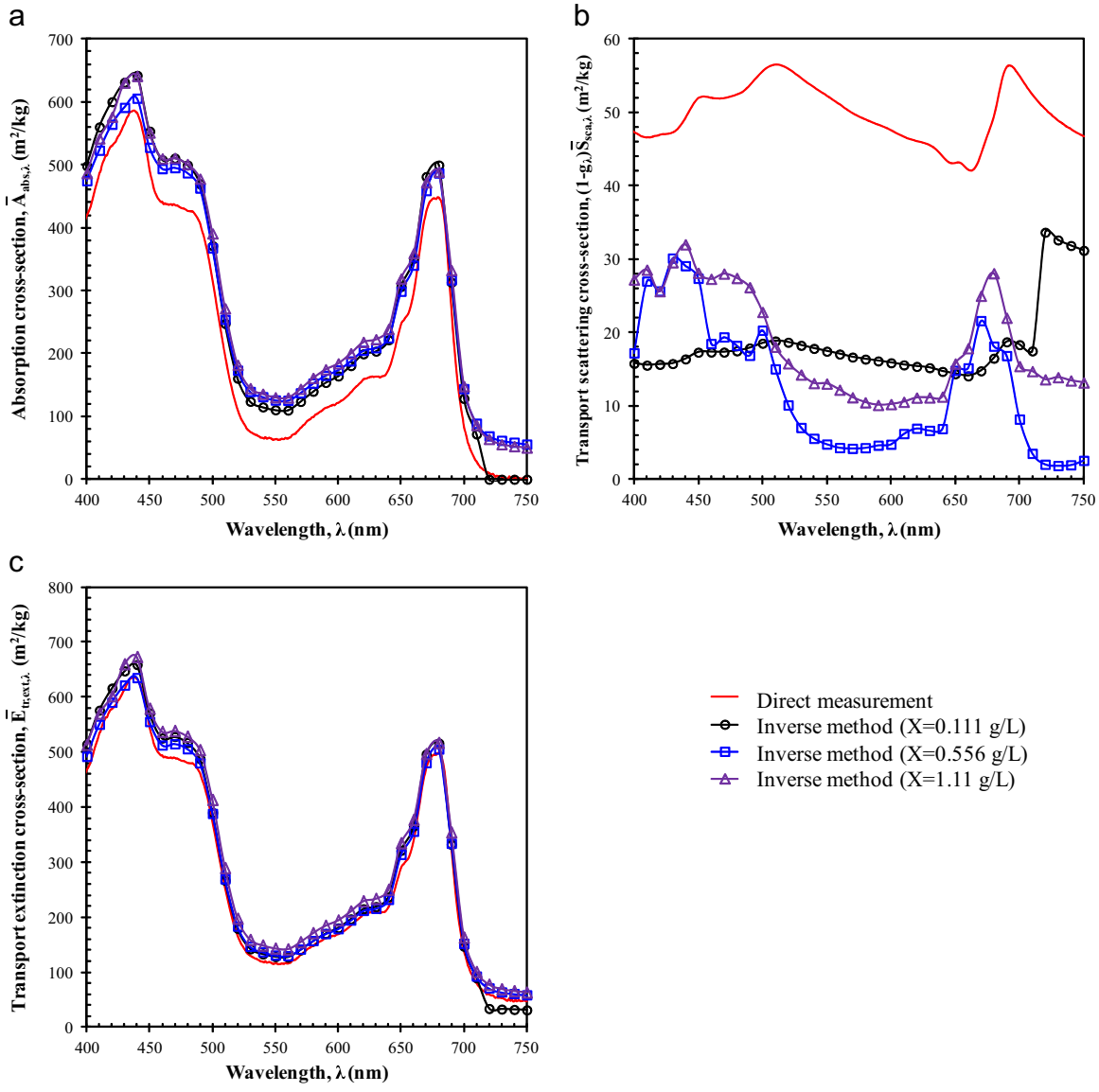

Fig. 7. Retrieved average spectral mass (a) absorption $\overline{A}_{abs,\lambda}$, (b) transport scattering $(1-g_\lambda)\overline{S}_{sca,\lambda}$, and (c) transport extinction $\overline{E}_{tr,ext,\lambda}$ cross-sections of *C. vulgaris* suspensions between 400 and 750 nm for biomass concentrations X of 0.111, 0.556, and 1.11 g/L.

(1) the radiation transfer in cuvettes containing microalgae cultures can be treated as one-dimensional and (2) the modified two-flux approximation is an adequate model for predicting the associated normal–hemispherical transmittance and reflectance. Note that the transmittance was underpredicted and reflectance was overpredicted at wavelengths between 500 nm and 600 nm. This may be due to the fact that the asymmetry factor g_λ was assumed to be constant over the PAR region. In fact, the spectral asymmetry factor g_λ of *C. vulgaris* can vary by as much as 80% over the PAR region relative to its value at 633 nm (Dauchet, 2012). Moreover, the use of transport approximation may have also contributed to the inaccuracy in the predicted transmittance and reflectance, particularly at higher cell concentrations. Indeed, Dombrovsky et al. (2005) state that "the error of the transport approximation increases with optical thickness but it is insignificant in the range of weak extinction".

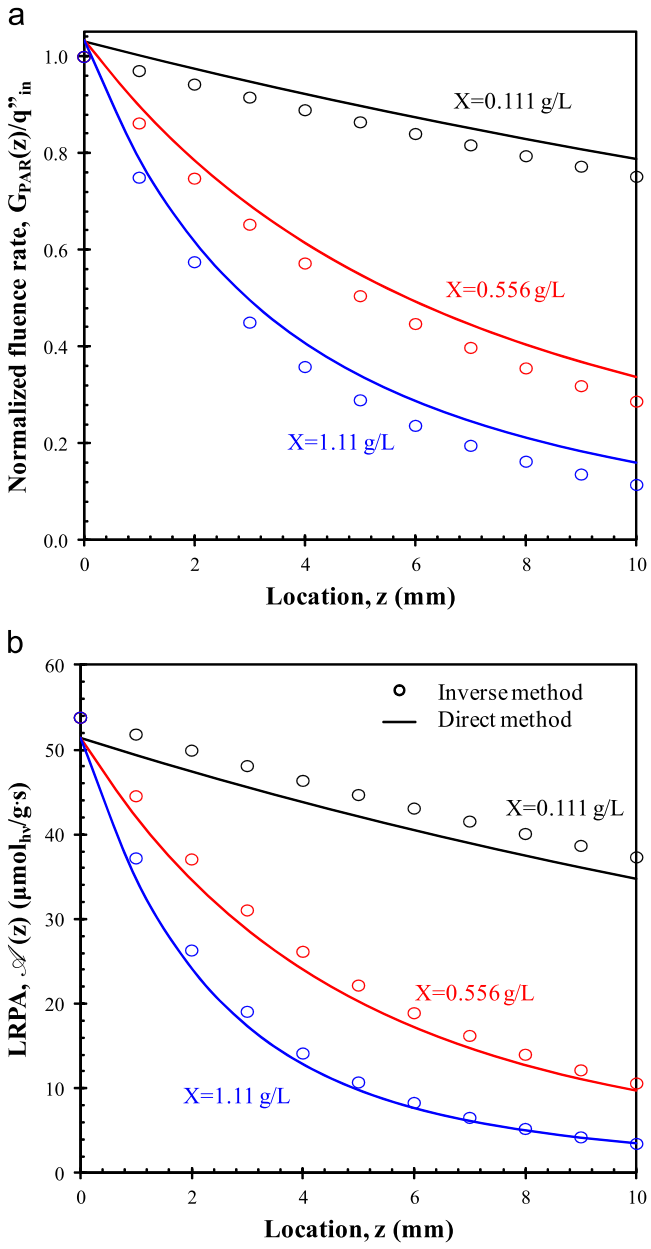

Fig. 8. Comparison of (a) fluence rate ratio $G_{PAR}(z)/q''_{in}$ and (b) local rate of photon absorption (LRPA) $\mathscr{A}(z)$ as a function of depth in a 1 cm thick flat plate PBR predicted by Eqs. (8) and (16), respectively. The predictions used the radiation characteristics obtained from either direct measurements or retrieved by the inverse method for concentrations 0.111, 0.556, and 1.11 g/L.

5.3.3. Retrieved cross-sections

Fig. 7 compares the average mass (a) absorption $\overline{A}_{abs,\lambda}$, (b) transport scattering $(1-g_\lambda)\overline{S}_{sca,\lambda}$, and (c) transport extinction $\overline{E}_{tr,ext,\lambda}=\overline{A}_{abs,\lambda}+(1-g_\lambda)\overline{S}_{sca,\lambda}$ cross-sections as functions of wavelength between 400 and 750 nm either measured directly or retrieved by the inverse method from measurements of $T_{nh,\lambda}$ and $R_{nh,\lambda}$ for three different concentrations. First, the retrieved spectral average mass absorption cross-section $\overline{A}_{abs,\lambda}$ was similar for each biomass concentration, as expected from its definition (Eq. (6)). In addition, the values of $\overline{A}_{abs,\lambda}$ retrieved by the inverse method were in relatively good agreement with those obtained from direct measurements except above 700 nm where it should vanish. Note that the inverse method retrieved $\overline{A}_{abs,\lambda}$ for each wavelength independently. Yet, the retrieved spectral absorption cross-section $\overline{A}_{abs,\lambda}$ was a continuous and smooth function of wavelength. On the other hand, the retrieved transport scattering

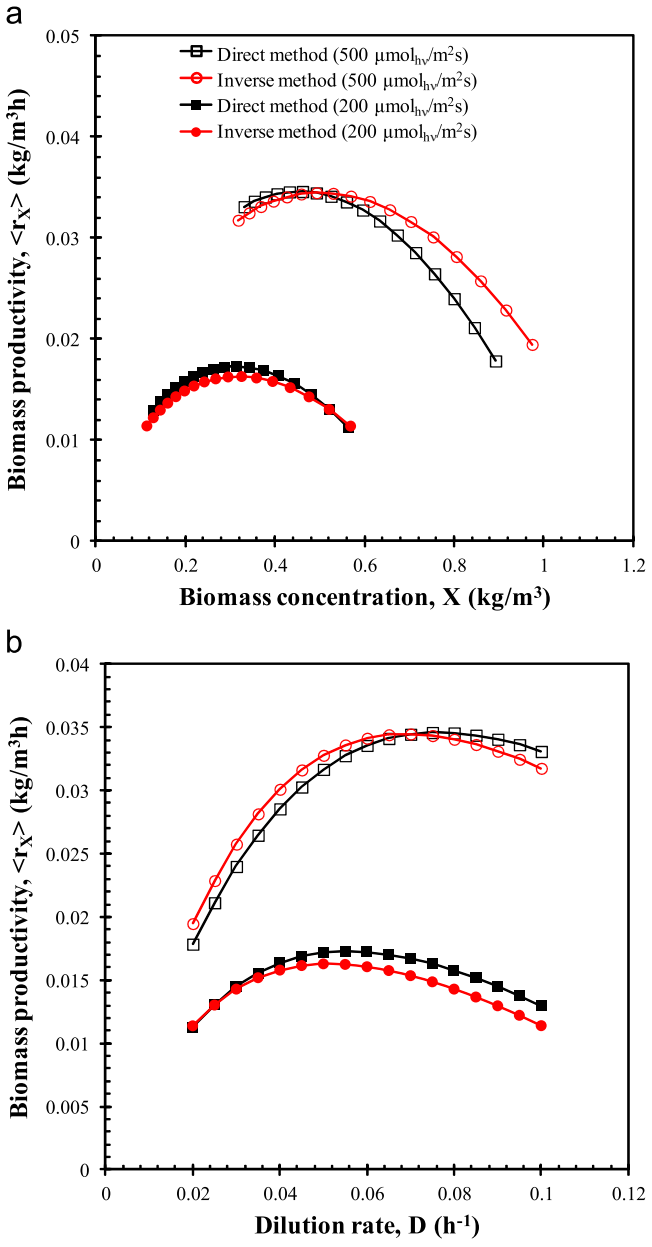

Fig. 9. Comparison of biomass productivity $\langle r_X \rangle$ of *C. vulgaris* grown in a 1 cm thick flat-plate PBRs exposed to 200 or 500 $\mu mol_{h\nu}/m^2$ s incident white LED light, predicted using Eqs. (12)–(16) as a function of either (a) the steady-state biomass concentration X or (b) the dilution rate D. The predictions used the radiation characteristics obtained from either direct measurements or retrieved by the inverse method.

cross-section $(1-g_\lambda)\overline{S}_{sca,\lambda}$ depended on the concentration considered and featured non-physical fluctuations as a function of wavelength. It was also significantly smaller than the values obtained from direct measurements. Finally, excellent agreement was found between all three retrieved transport extinction cross-sections $\overline{E}_{tr,ext,\lambda}$ and the experimentally measured one. Note that the inverse method overestimated the value of $\overline{A}_{abs,\lambda}$ and compensated for it by underpredicting the transport scattering cross-section $(1-g_\lambda)\overline{S}_{sca,\lambda}$ of the microorganisms. This was due to the fact that normal–hemispherical transmittance $T_{nh,\lambda}$ and reflectance $R_{nh,\lambda}$ measurements of microalgae were not very sensitive to the cells' transport scattering cross-section as microalgae scattered light mainly in the forward direction. In addition, the forward scattered light was collected by the integrating sphere used in the measurements of $T_{nh,\lambda}$. In fact, the absorption cross-section dominated over the transport scattering cross-section (i.e., $\overline{A}_{abs,\lambda} \gg (1-g_\lambda)\overline{S}_{sca,\lambda}$) so that small errors in $\overline{A}_{abs,\lambda}$ had strong effects on the shape and magnitude of the transport scattering cross-section $(1-g_\lambda)\overline{S}_{sca,\lambda}$. This was confirmed by the fact that good agreement was observed between the direct and inverse methods for the transport extinction cross-section $\overline{E}_{tr,ext,\lambda}$.

Moreover, the same inverse procedure and algorithm was used to retrieve the three parameters $\overline{A}_{abs,\lambda}$, $\overline{S}_{sca,\lambda}$, and g_λ independently. This resulted in strongly oscillating values of $\overline{S}_{sca,\lambda}$ and g_λ. However, the same values of $\overline{A}_{abs,\lambda}$ and $(1-g_\lambda)\overline{S}_{sca,\lambda}$ as those shown in Fig. 7 were obtained. This can be attributed to the facts that (i) the solution of the ill-posed inverse problem was not unique and (ii) the modified two-flux approximation for the expressions of $T_{nh,\lambda,pred}$ and $R_{nh,\lambda,pred}$ depended on the transport scattering coefficient $\sigma_{s,tr,\lambda}$ and not on $\sigma_{s,\lambda}$ and g_λ separately.

As argued earlier, the average mass absorption cross-section $\overline{A}_{abs,\lambda}$ is the most important radiation characteristic in analyzing, predicting, and controlling coupled light transfer and growth kinetics in PBRs. In fact, Fig. 8a shows the fluence rate ratio $G_{PAR}(z)/q''_{in}$ in a 1 cm thick flat plate PBR illuminated normally on one side with a front transparent window and a back reflectivity $\rho_\lambda = 0.02$. The fluence rate ratio was predicted by using either (i) the two-flux approximation given by Eq. (8) based on the directly measured radiation characteristics $\overline{A}_{abs,\lambda}$ and $\overline{S}_{sca,\lambda}$ with $b_\lambda = 0.0042$ or (ii) the simplified two-flux approximation given by Eq. (11) based on the retrieved values of $\overline{A}_{abs,\lambda}$ for concentrations 0.111, 0.556, and 1.11 g/L.

Fig. 8b compares the local rate of photon absorption (LRPA) $\mathcal{A}(z)$ as a function of flat plate PBR thickness predicted by Eq. (16) using the fluence rate shown in Fig. 8a and the associated absorption and scattering cross-sections. Here, the light source was assumed to be collimated white LEDs delivering a total incident flux of 200 $\mu mol_{h\nu}/m^2$ s as previously used experimentally (Soulies et al., 2016). Fig. 8 indicates that the absorption cross-section retrieved by the inverse method combined with the simplified two-flux approximation (Eq. (11)) led to acceptable predictions of the fluence rate $G_{PAR}(z)$ and of the LRPA $\mathcal{A}(z)$. This was achieved while requiring fewer experimental measurements and only an integrating sphere spectrophotometer.

Finally, Fig. 9a and b shows the volume averaged steady-state biomass productivity $\langle r_X \rangle$ of *C. vulgaris* as a function of steady-state biomass concentration X and dilution rate D, respectively. Productivity was predicted using Eqs. (12)–(16) combined with either (i) the two-flux approximation given by Eq. (8) and the directly measured radiation characteristics $\overline{A}_{abs,\lambda}$, $\overline{S}_{sca,\lambda}$ with $b_\lambda = 0.0042$ or (ii) the simplified two-flux approximation given by Eq. (11) and the retrieved values of $\overline{A}_{abs,\lambda}$. A torus type 4 cm thick flat-plate PBR in continuous mode was simulated exposed to 200 or 500 $\mu mol_{h_\nu}/m^2$ s of collimated white LEDs and the dilution rate D varied from 0.02 to 0.1 h^{-1} as previously used experimentally (Soulies et al., 2016). Fig. 9 illustrates that the productivity predicted using the fluence rate estimated with the simplified two-flux approximation and the absorption cross-section retrieved by the inverse method was very similar to productivity predictions using the fluence rate estimated by the two-flux approximation and the directly measured radiation characteristics. Indeed, the relative difference between these two methods was less than 10% for all dilution rates D investigated and for both realistic incident irradiances considered.

6. Conclusion

This paper presented a method to easily measure the spectral absorption cross-section of randomly oriented microalgae of any shape from conventional normal–hemispherical transmittance and reflectance measurements of well-mixed suspensions in conventional cuvettes. It was successfully demonstrated with suspension of *C. vulgaris* with relatively large biomass concentrations such that multiple scattering prevailed. Even though the method was unable to properly retrieve the transport scattering cross-section, the retrieval of the absorption cross-section combined with the simplified two-flux approximation was sufficient to predict accurately the local fluence rate, the local rate of photon absorption, and the biomass productivity of flat plate PBRs. This new method can also be applied to other absorbing and scattering particles of various shapes with large enough size parameter to ensure strong forward scattering and therefore a small transport scattering cross-section compared with the absorption cross-section.

Acknowledgement

This work was supported by the French National Research Agency project DIESALG (ANR-12-BIME-0001-02) for biodiesel production based on solar production of microalgae, and is part of the French "BIOSOLIS" research program on developing photobioreactor technologies for mass-scale solar production (http://www.biosolis.org/). Additional support was provided by the CNRS program Cellule énergie. R.K. is grateful to the Embassy of France in the United States, Office for Science and Technology for the Chateaubriand Fellowship. L.P. thanks the Région Pays de la Loire for the Research Chair for International Junior Scientists.

Appendix A. Supplementary data

Supplementary data associated with this paper can be found in the online version at http://dx.doi.org/10.1016/j.ces.2016.02.039.

References

Agrawal, B.M., Mengüç, M.P., 1991. Forward and inverse analysis of single and multiple scattering of collimated radiation in an axisymmetric system. Int. J. Heat Mass Transf. 34, 633–647.

Bellini, S., Bendoula, R., Latrille, E., Roger, J.-M., 2014. Potential of a spectroscopic measurement method using adding-doubling to retrieve the bulk optical properties of dense microalgal media. Appl. Spectrosc. 68 (October (10)), 1154–1167.

Berberoğlu, H., Pilon, L., 2007. Experimental measurement of the radiation characteristics of *Anabaena variabilis* ATCC 29413-U and *Rhodobacter sphaeroides* ATCC 49419. Int. J. Hydrog. Energy 32, 4772–4785.

Berberoğlu, H., Yin, J., Pilon, L., 2007. Light transfer in bubble sparged photobioreactors for H_2 production and CO_2 mitigation. Int. J. Hydrog. Energy 32, 2273–2285.

Berberoğlu, H., Melis, A., Pilon, L., 2008. Radiation characteristics of *Chlamydomonas reinhardtii* CC125 and its truncated chlorophyll antenna transformants *tla1*, *tlaX*, and *tla1-CW*$^+$. Int. J. Hydrog. Energy 33, 6467–6483.

Berberoğlu, H., Gomez, P.S., Pilon, L., 2009. Radiation characteristics of *Botryococcus braunii*, *Chlorococcum littorale*, and *Chlorella sp* used for CO_2 fixation and biofuel production. J. Quant. Spectrosc. Radiat. Transf. 110, 1879–1893.

Bidigare, R., Ondrusek, M., Morrow, J., Kiefer, D., 1990. In vivo absorption properties of algal pigments. Ocean Opt. X 1302, 290–301.
Brennan, L., Owende, P., 2013. Biofuels from microalgae: towards meeting advanced fuel standards. In: Lee, James W. (Ed.), Advanced Biofuels and Bioproducts. Springer, New York, pp. 553–599.
Charbonneau, P., Knapp, B., 1995. A User's Guide to PIKAIA 1.0. Technical Report, NCAR Technical Note 418+IA, National Center for Atmospheric Research.
Charbonneau, P., 2002. An Introduction to Genetic Algorithms for Numerical Optimization. Technical Report, NCAR Technical Note 450+IA, National Center for Atmospheric Research.
Charbonneau, P., 2002. Release Notes for PIKAIA 1.2. Technical Report, NCAR Technical Note 451+STR, National Center for Atmospheric Research.
Cornet, J.F., Dussap, C.G., 2009. A simple and reliable formula for assessment of maximum volumetric productivities in photobioreactors. Biotechnol. Prog. 25, 424–435.
Cornet, J.-F., Dussap, C.G., Dubertret, G., 1992. A structured model for simulation of cultures of the cyanobacterium *Spirulina platensis* in photobioreactors: I. Coupling between light transfer and growth kinetics. Biotechnol. Bioeng. 40, 817–825.
Cornet, J.-F., Dussap, C.G., Cluzel, P., Dubertret, G., 1992. A structured model for simulation of cultures of the cyanobacterium *Spirulina platensis* in photobioreactors: II. Identification of kinetic parameters under light and mineral limitations. Biotechnol. Bioeng. 40, 826–834.
Cornet, J.-F., Dussap, C.G., Gross, J.B., Binois, C., Lasseur, C., 1995. A simplified monodimensional approach for modeling coupling between radiant light transfer and growth kinetics in photobioreactors. Chem. Eng. Sci. 50, 1489–1500.
Cornet, J.-F., Dussap, C.G., Gros, J.-B., 1998. Kinetics and energetics of photosynthetic micro-organisms in photobioreactors. In: Bioprocess and Algae Reactor Technology, Apoptosis, Advances in Biochemical Engineering Biotechnology, vol. 59. Springer, Berlin, Heidelberg, pp. 153–224.
Dauchet, J., Blanco, S., Cornet, J.-F., Fournier, R., 2015. Calculation of the radiative properties of photosynthetic microorganisms. J. Quant. Spectrosc. Radiat. Transf. 161, 60–84.
Dauchet, J., 2012. Analyse Radiative des Photobioréacteurs (Ph.D. thesis). Université Blaise Pascal, Clermont Ferrand II, France.
Davies-Colley, R.J., Pridmore, R.D., Hewitt, J.E., 1986. Optical properties of some freshwater phytoplanktonic algae. Hydrobiologia 133, 165–178.
Dombrovsky, L., Randrianalisoa, H., Baillis, D., Pilon, L., 2005. Use of Mie theory to analyze experimental data to identify infrared properties of fused quartz containing bubbles. Appl. Opt. 44 (33), 7021–7031.
Feng, Y., Li, C., Zhang, D., 2011. Lipid production of *Chlorella vulgaris* cultured in artificial wastewater medium. Bioresour. Technol. 102 (1), 101–105.
Fouchard, S., Pruvost, J., Degrenne, B., Titica, M., Legrand, J., 2009. Kinetic modeling of light limitation and sulfur deprivation effects in the induction of hydrogen production with *Chlamydomonas reinhardtii*: part I. Model development and parameter identification. Biotechnol. Bioeng. 102, 232–245.
Griffiths, M.J., Harrison, S.T.L., 2009. Lipid productivity as a key characteristic for choosing algal species for biodiesel production. J. Appl. Phycol. 21 (5), 493–507.
Heng, R.-L., Pilon, L., 2014. Time-dependent radiation characteristics of *Nannochloropsis oculata* during batch culture. J. Quant. Spectrosc. Radiat. Transf. 144, 154–163.
Heng, R.-L., Lee, E., Pilon, L., 2014. Radiation characteristics and optical properties of filamentous cyanobacteria *Anabaena cylindrica*. J. Opt. Soc. Am. A 31 (4), 836–845.
Heng, R.-L., Sy, K.C., Pilon, L., 2015. Absorption and scattering by bispheres, quadspheres, and circular rings of spheres and their equivalent coated spheres. J. Opt. Soc. Am. A 32 (1), 46–60.
Heraeus, 2015. Quartz glass for optics: data and properties, ⟨http://www.heraeus-quarzglas.com/media/webmedia_local/downloads/broschren_mo/DataandProperties_Optics_fusedsilica.pdf⟩.
Kandilian, R., Lee, E., Pilon, L., 2013. Radiation and optical properties of *Nannochloropsis oculata* grown under different irradiances and spectra. Bioresour. Technol. 137, 63–73.
Kandilian, R., Pruvost, J., Legrand, J., Pilon, L., 2014. Influence of light absorption rate by *Nannochloropsis oculata* on triglyceride production during nitrogen starvation. Bioresour. Technol. 163, 308–319.
Kandilian, R., Tsao, T.-C., Pilon, L., 2014. Control of incident irradiance on a batch operated flat-plate photobioreactor. Chem. Eng. Sci. 119, 99–108.
Kandilian, R., Heng, R.-L., Pilon, L., 2015. Absorption and scattering by fractal aggregates and by their equivalent coated spheres. J. Quant. Spectrosc. Radiat. Transf. 151, 310–326.
Kong, B., Vigil, R.D., 2014. Simulation of photosynthetically active radiation distribution in algal photobioreactors using a multidimensional spectral radiation model. Bioresour. Technol. 158, 141–148.
Lee, E., Pilon, L., 2013. Absorption and scattering by long and randomly oriented linear chains of spheres. J. Opt. Soc. Am. A 30 (9), 1892–1900.
Lee, E., Pruvost, J., He, X., Munipalli, R., Pilon, L., 2014. Design tool and guidelines for outdoor photobioreactors. Chem. Eng. Sci. 106, 18–29.
McKellar, B.H.J., Box, M.A., 1981. The scaling group of the radiative transfer equation. J. Atmos. Sci. 38 (5), 1063–1068.
Mendes, R.L., Nobre, B.P., Cardoso, M.T., Pereira, A.P., Palavra, A.F., 2003. Supercritical carbon dioxide extraction of compounds with pharmaceutical importance from microalgae. Inorg. Chim. Acta 356, 328–334.
Modest, M.F., 2013. Radiative Heat Transfer, third ed. Elsevier, Oxford, UK.
Murphy, T.E., Berberoğlu, H., 2011. Effect of algae pigmentation on photobioreactor productivity and scale-up: a light transfer perspective. J. Quant. Spectrosc. Radiat. Transf. 112, 2826–2834.
Pilon, L., Berberoğlu, H., Kandilian, R., 2011. Radiation transfer in photobiological carbon dioxide fixation and fuel production by microalgae. J. Quant. Spectrosc. Radiat. Transf. 112, 2639–2660.
Pilon, L., 2015. Excel spreadsheet for retrieving the spectral absorption cross-section from normal–hemispherical reflectance and transmittance, ⟨http://repositories.cdlib.org/escholarship/⟩ or ⟨http://www.seas.ucla.edu/pilon/downloads.htm⟩ (accessed 15.06.15).
Pires, J.C.M., 2015. Chapter 5 – mass production of microalgae. In: Kim, Se-Kwon (Ed.), Handbook of Marine Microalgae. Academic Press, Boston, pp. 55–68.
Pottier, L., Pruvost, J., Deremetz, J., Cornet, J.-F., Legrand, J., Dussap, C.G., 2005. A fully predictive model for one-dimensional light attenuation by *Chlamydomonas reinhardtii* in a torous photobioreactor. Biotechnol. Bioeng. 91, 569–582.
Prahl, S.A., Van Gemert, M.J.C., Welch, A.J., 1993. Determining the optical properties of turbid media by using the adding-doubling method. Appl. Opt. 32 (4), 559–568.
Privoznik, K.G., Daniel, K.J., Incropera, F.P., 1978. Absorption,extinction, and phase function measurements for algal suspensions of *Chlorella pyrenoidosa*. J. Quant. Spectrosc. Radiat. Transf. 20, 345–352.
Pruvost, J., Cornet, J.F., Goetz, V., Legrand, J., 2012. Theoretical investigation of biomass productivities achievable in solar rectangular photobioreactors for the cyanobacterium *Arthrospira platensis*. Biotechnol. Prog. 28, 699–714.
Pruvost, J., Le Gouic, B., Lepine, O., Legrand, J., Le Borgne, F., 2016. Microalgae culture in building-integrated photobioreactors: biomass production modelling and energetic analysis. Chem. Eng. J. 284, 850–861.
Richmond, A., 2004. Handbook of Microalgal Culture. Blackwell Science Ltd, Oxford, UK.
Ritchie, R., 2006. Consistent sets of spectrophotometric chlorophyll equations for acetone, methanol and ethanol solvents. Photosynth. Res. 89, 27–41.
Safi, C., Zebib, B., Merah, O., Pontalier, P.-Y., Vaca-Garcia, C., 2014. Morphology, composition, production, processing and applications of *Chlorella vulgaris*: a review. Renew. Sustain. Energy Rev. 35, 265–278.
Soulies, A., Pruvost, J., Castelain, C., Burghelea, T.I., Legrand, J., 2016. Investigation and modeling of the effects of light spectrum and incident angle on *Chlorella vulgaris* in photobioreactors. Biotechnol. Prog. (in press)
Stramski, D., Piskozub, J., 2003. Estimation of scattering error in spectrophotometric measurements of light absorption by aquatic particles from three-dimensional radiative transfer simulations. Appl. Opt. 42 (18), 3634–3646.
Strickland, J.D., Parsons, T.R., 1968. A Practical Handbook of Seawater Analysis. Fisheries Research Board of Canada, Ottawa, Canada.
Takache, H., Christophe, G., Cornet, J.-F., Pruvost, J., 2010. Experimental and theoretical assessment of maximum productivities for the microalgae *Chlamydomonas reinhardtii* in two different geometries of photobioreactors. Biotechnol. Prog. 26 (2), 431–440.
Takache, H., Pruvost, J., Cornet, J.-F., 2012. Kinetic modeling of the photosynthetic growth of *Chlamydomonas reinhardtii* in a photobioreactor. Biotechnol. Prog. 28 (3), 681–692.
Tokuşoglu, Ö, Ünal, M.K., 2003. Biomass nutrient profiles of three microalgae: *Spirulina platensis*, *Chlorella vulgaris*, and *Isochrisis galbana*. J. Food Sci. 68 (4), 1144–1148.
Van De Hulst, H.C., 1957. Light Scattering by Small Particles. Wiley, New York, NY.
Wheaton, Z.C., Krishnamoorthy, G., 2012. Modeling radiative transfer in photobioreactors for algal growth. Comput. Electron. Agric. 87, 64–73.